Spatially Tunable Spin Interactions in Neutral Atom Arrays

Lea-Marina Steinert,[1,2,3,*] Philip Osterholz,[1,2,3] Robin Eberhard,[1,2] Lorenzo Festa,[1,2] Nikolaus Lorenz,[1,2] Zaijun Chen,[1,2] Arno Trautmann,[1,2,3] and Christian Gross[1,2,3]

[1]*Max-Planck-Institut für Quantenoptik, 85748 Garching, Germany*
[2]*Munich Center for Quantum Science and Technology (MCQST), 80799 München, Germany*
[3]*Physikalisches Institut, Eberhard Karls Universität Tübingen, 72076 Tübingen, Germany*

(Received 2 November 2022; revised 20 January 2023; accepted 16 May 2023; published 16 June 2023)

Analog quantum simulations with Rydberg atoms in optical tweezers routinely address strongly correlated many-body problems due to the hardware-efficient implementation of the Hamiltonian. Yet, their generality is limited, and flexible Hamiltonian-design techniques are needed to widen the scope of these simulators. Here we report on the realization of spatially tunable interactions for XYZ models implemented by two-color near-resonant coupling to Rydberg pair states. Our results demonstrate the unique opportunities of Rydberg dressing for Hamiltonian design in analog quantum simulators.

DOI: 10.1103/PhysRevLett.130.243001

Quantum simulators based on arrays of neutral atoms have proven to be among the most promising platforms to address nontrivial problems of strongly correlated many-body phenomena. This success is based on the optimally hardware-efficient analog implementation of the Hamiltonian under study [1–4], which is one of the reasons to employ these machines for useful tasks in the so-called NISQ (noisy intermediate-scale quantum) era of quantum processors. While such an emulation approach eliminates any overhead in control necessities or qubit numbers, it strongly restricts the use cases of a specific quantum simulator to problems rooted in the device-dependent Hamiltonian. Here, neutral atoms trapped in optical tweezer arrays with engineered geometries in two dimensions, laser coupled to Rydberg states to induce interactions [5], are among the most promising platforms [6–12]. Large system sizes have been demonstrated with long coherence times [12,13], enabling the simulation of quantum magnets both in equilibrium [14,15] and dynamically [16].

Rydberg atom-based simulators naturally implement Ising or XY-type Hamiltonians with power-law interactions [17–20]. Recently, Floquet-engineered XXZ spin coupling in bulk systems and optical tweezer arrays has been demonstrated [21,22]. Control over the spatial interaction profile of Ising systems has been realized by admixing Rydberg character to the ground state, so-called Rydberg dressing [23–30]. Lately, a sharply peaked interaction profile has been demonstrated by coupling to molecular Rydberg macrodimer potentials [31]. One of the biggest remaining challenges is to increase the systems' flexibility via universally programmable analog qubit couplings.

We report on progress into this direction by the realization of freely tunable short-range XYZ-type spin interactions between atoms trapped in optical tweezer arrays. The effective spin-1/2 system is encoded in two electronic ground states. We introduce interactions by two-color Rydberg dressing, which allows us to engineer the spin-spin couplings in each spin direction by the choice of the laser parameters. Our approach uses the spatially dependent van-der-Waals (vdW) interactions between different m_j sublevels in the Rydberg pair state manifold to design distance and angular-dependent couplings of the XYZ Hamiltonian [33]

$$\hat{H}_{XYZ} = \hbar \sum_{i<j} (J_{ij}^{z} \hat{\sigma}_i^{z} \hat{\sigma}_j^{z} + J_{ij}^{++} \hat{\sigma}_i^{+} \hat{\sigma}_j^{+} + J_{ij}^{+-} \hat{\sigma}_i^{+} \hat{\sigma}_j^{-}) + \text{H.c.} \tag{1}$$

The Pauli matrices $\hat{\sigma}_j^{z}$, $\hat{\sigma}_j^{x} = (\hat{\sigma}_j^{+} + \hat{\sigma}_j^{-})$ and $\hat{\sigma}_j^{y} = i(\hat{\sigma}_j^{-} - \hat{\sigma}_j^{+})$ describe a spin-1/2 particle at position j. This Hamiltonian distinguishes between three types of spin couplings J_{ij}^{γ}: the diagonal interaction between dressed ground states J_{ij}^{z}, the off-diagonal "flop-flop" J_{ij}^{++}, and "flip-flop" J_{ij}^{+-} interactions. While dressing-induced Ising (J^z) interactions have already been studied in various experiments [26,27,30,31,34–36] and programmable long-range interactions have been demonstrated in optical cavities [37], we focus on programmable J_{ij}^{++} and J_{ij}^{+-} interactions (Fig. 1). With control over the laser parameters and the geometric arrangement of single atoms,

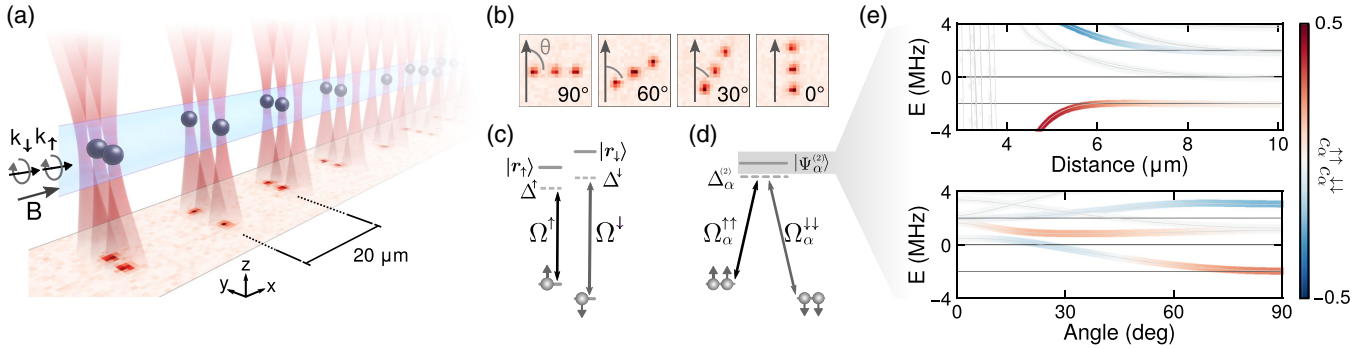

FIG. 1. Experimental setup and level schemes. (a) Illustration of the experimental setting. The Rydberg excitation beams ($\mathbf{k}_\uparrow$, $\mathbf{k}_\downarrow$, light blue) are aligned along the magnetic field $\mathbf{B}$, driving σ^- transitions. They illuminate all tweezer groups, each with three linearly arranged tweezers (red), which are statistically loaded with atoms (black spheres). At the bottom of the illustration, a single shot fluorescence image is shown. (b) Exemplary images for various angles θ at a distance of 5.2 μm. (c) On the single-atom level, we couple the electronic ground states ($|\uparrow\rangle$, $|\downarrow\rangle$) to the Rydberg states ($|r_\uparrow\rangle$, $|r_\downarrow\rangle$) with Rabi frequencies ($\Omega^\uparrow, \Omega^\downarrow$) and detunings ($\Delta^\uparrow, \Delta^\downarrow$). (d) Schematic for the flop-flop interaction J_{ij}^{++} between two atoms i and j. Via adiabatic elimination of the singly excited pair states, we reduce the four-photon process to an effective Λ scheme. The pairs of ground state atoms are coupled with the effective Rabi couplings ($\Omega_\alpha^{\uparrow\uparrow}, \Omega_\alpha^{\downarrow\downarrow}$) to Rydberg pair states $|\Psi_\alpha^{(2)}\rangle$. $\Delta_\alpha^{(2)}$ is the two-photon detuning to each $|\Psi_\alpha^{(2)}\rangle$, which includes interaction induced shifts. (e) Calculated eigenenergies of $\hat{H}_{\mathrm{Ryd}}$ depending on the atom pair distance d at an angle of $\theta = 90°$ (upper) and atom pair angle θ at a distance $d = 6$ μm (lower). The color scale corresponds to the overlap $c_\alpha^{\uparrow\uparrow} c_\alpha^{\downarrow\downarrow}$. The solid lines at ±2 MHz mark the energy of the asymptotic Rydberg pair state ($|r_\downarrow r_\downarrow\rangle$, $|r_\uparrow r_\uparrow\rangle$). The theoretical results are obtained by exact diagonalization of H_{Ryd} using the PAIRINTERACTION software package [32].

we can engineer the relative coupling strength of the spin-spin interactions J_{ij}^{++}/J_{ij}^{z} and J_{ij}^{+-}/J_{ij}^{z} as visualized exemplarily in Fig. 2. We are also able to switch off specific couplings globally by the choice of the laser detunings as discussed below. In a 2D configuration, the situation is even more complex: the angular dependence of the interaction provides a unique opportunity to control the nearest-neighbor versus longer-ranged interaction and to realize

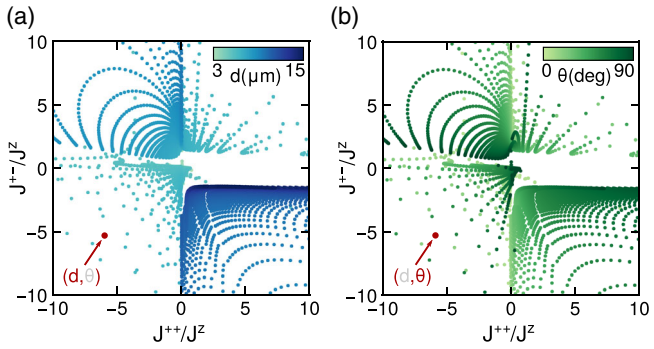

FIG. 2. Tunable XYZ interactions in 1D chains. Both panels show the same calculation, highlighting the distance (a) and angle (b) dependence of the ratios J_{ij}^{++}/J_{ij}^{z} and J_{ij}^{+-}/J_{ij}^{z} for one set of detunings $(\Delta^\uparrow, \Delta^\downarrow) = 2\pi \cdot (1.4, -0.6)$ MHz. The interactions are calculated in steps of 100 nm and 1°. Quadrants II and IV show a smooth tunability, while the ratios in quadrants I and III are realized close to Rydberg pair state resonances. The latter requires higher stability of the control parameters, but may ultimately be beneficial for the achievable coherence [38].

models featuring various magnetic phenomena, including frustration and topology [7,10,33,38–40]. Our approach also opens new pathways to quantum simulations with practical relevance for the inference of Hamiltonians underlying spectra obtained in nuclear magnetic resonance experiments in chemistry and biology [41].

The physical system we use is an optical tweezer array of single ^{39}K atoms. The spins are encoded in the hyperfine states $|\uparrow\rangle = |4S_{1/2}F = 2, m_F = -2\rangle$ and $|\downarrow\rangle = |4S_{1/2}F = 1, m_F = -1\rangle$. Both states are coupled individually to the Rydberg states $|r_\uparrow\rangle = |62P_{3/2}, m_j = -3/2\rangle$ and $|r_\downarrow\rangle = |62P_{3/2}, m_j = -1/2\rangle$ by off-resonant single photon excitation with Rabi frequencies ($\Omega^\uparrow, \Omega^\downarrow$), and detunings ($\Delta^\uparrow, \Delta^\downarrow$) (Fig. 1). The choice of beam polarizations suppresses single-atom Raman couplings. In this doubly laser-coupled system, rich spin-spin interactions emerge, which are rooted in the strong vdW interactions between the addressed Rydberg pair states. For the derivation of the spin couplings J_{ij}^{++} and J_{ij}^{+-}, we start with diagonalizing $\hat{H}_{\mathrm{Ryd}} = \hat{H}_{\mathrm{las}} + \hat{H}_{\mathrm{int}}$ in the Rydberg pair state basis [33]. Here, $\hat{H}_{\mathrm{las}}$ is the single atom Hamiltonian in the rotating frame. The vdW Hamiltonian $\hat{H}_{\mathrm{int}}$ leads to interactions between the different m_j levels in the $62P_{3/2}$ manifold. We admix different components of the vdW pair eigenstates to the ground states by laser coupling to obtain the effective interactions between the ground states.

The interactions in Eq. (1) can be understood as four-photon processes by adiabatic elimination of all excited states [33,42]. For example, for the flop-flop interactions, the coupling of the $|\uparrow\uparrow\rangle$ pair ground state to a Rydberg pair

eigenstate $|\Psi_\alpha^{(2)}\rangle$ follows by adiabatic elimination of the singly excited state as $\Omega_\alpha^{\uparrow\uparrow} = (\Omega^\uparrow)^2 \cdot c_\alpha^{\uparrow\uparrow}/2\Delta^\uparrow$, where $c_\alpha^{\uparrow\uparrow} = \langle\Psi_\alpha^{(2)}|r^\uparrow r^\uparrow\rangle$ is the wave function overlap of one eigenstate $|\Psi_\alpha^{(2)}\rangle$ in the Rydberg manifold with the asymptotic Rydberg pair state $|r^\uparrow r^\uparrow\rangle$. The coupling of $|\downarrow\downarrow\rangle$ follows analogously. For sufficiently large detuning of the lasers to any coupled state in the Rydberg manifold, we eliminate the Rydberg pair eigenstates to arrive at an effective coupling between ground state atom pairs i and j:

$$J_{ij}^{++} = 2\sum_\alpha \frac{\Omega_\alpha^{\uparrow\uparrow}\Omega_\alpha^{\downarrow\downarrow}}{\Delta_\alpha^{(2)}} = \frac{(\Omega^\uparrow\Omega^\downarrow)^2}{4\Delta^\uparrow\Delta^\downarrow} \cdot \frac{c_\alpha^{\uparrow\uparrow}c_\alpha^{\downarrow\downarrow}}{\Delta_\alpha^{(2)}}. \quad (2)$$

The Rydberg pair state detuning $\Delta_\alpha^{(2)}$ includes vdW interaction-induced shifts $U_{\mathrm{vdW},\alpha}$. Spin flips from $|\uparrow\uparrow\rangle$ to $|\downarrow\downarrow\rangle$ and vice versa require a nonzero probability overlap $c_\alpha^{\uparrow\uparrow}c_\alpha^{\downarrow\downarrow}$ provided by the mixing of the m_j sublevels.

The derivation of J_{ij}^{+-} starts with two atoms in opposite spin states ($|\uparrow\downarrow\rangle$,$|\downarrow\uparrow\rangle$). Different from the flop-flop interaction case, there are two excitation paths to the Rydberg manifold. Via adiabatic elimination of the intermediate singly excited state we obtain an effective two-photon coupling $\Omega_\alpha^{\uparrow\downarrow} = \Omega^\uparrow\Omega^\downarrow \cdot c_\alpha^{\uparrow\downarrow} \cdot (1/4\Delta^\uparrow + 1/4\Delta^\downarrow)$. Then, in fourth order perturbation theory, we obtain the flip-flop interaction:

$$\begin{aligned} J_{ij}^{+-} &= 2\sum_\alpha \frac{\Omega_\alpha^{\uparrow\downarrow}\Omega_\alpha^{\downarrow\uparrow}}{\Delta_\alpha^{(2)}} \\ &= \sum_\alpha \frac{(\Omega^\uparrow\Omega^\downarrow)^2}{16(\Delta^\uparrow\Delta^\downarrow)^2} \cdot (\Delta^\uparrow + \Delta^\downarrow)^2 \cdot \frac{c_\alpha^{\downarrow\uparrow}c_\alpha^{\downarrow\uparrow}}{\Delta_\alpha^{(2)}}. \end{aligned} \quad (3)$$

For finite flip-flop interaction, we require a nonzero overlap of $c_\alpha^{\uparrow\downarrow}c_\alpha^{\downarrow\uparrow}$. In the case of symmetric detunings $\Delta^\uparrow = -\Delta^\downarrow$, the flip-flop interaction is generally canceled by destructive interference of the excitation paths. This provides us with sensitive control of J_{ij}^{+-} by choosing the excitation laser detuning accordingly. In contrast, energy conservation restricts the flop-flop processes and requires the laser detunings to be set to $\Delta^\uparrow - \Delta^\downarrow = E_z$, with E_z the Zeeman splitting between $|r^\uparrow\rangle$ and $|r^\downarrow\rangle$ [Fig. 3(c)].

To study the dependence of the interaction strengths on the geometric arrangement experimentally, we select the simplest possible setting of three in-line traps with various nearest-neighbor distances d and angles θ [Figs. 1(a) and 1(b)]. Here, θ is the angle between the interatomic separation vector $\mathbf{d}$ and the magnetic field $\mathbf{B}$, which is set to 1 G and defines the quantization axis. We use 14 replications of this pattern for increased statistics, where the intergroup spacing is 20 μm, larger than any interaction range in the system. With a first fluorescence image of the atom array, we check for the presence of an atom in the trap. We then prepare all atoms in the $|\uparrow\rangle$ state and perform

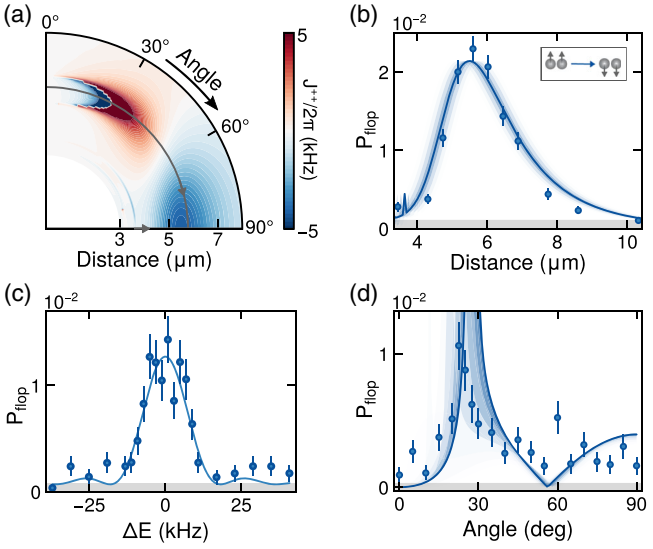

FIG. 3. Flop-flop interactions. (a) Calculation of J^{++} as a function of θ and d for $\Delta_\uparrow = -\Delta_\downarrow = 2\pi \cdot 1$ MHz. We identify a resonance in the spin-spin couplings appearing as a singularity around $\theta = 30°$ at a distance of 5–6 μm. (b) Observed flop-flop probability P_{flop} for different atom pair distances at $\theta = 90°$. A small false positive probability sets the detection limit (gray area) taking into account single spin flips and inefficient state preparation and push out. Error bars indicate 1 s.e.m. The solid line is the theoretical prediction, where the amplitude has been scaled to match the experimental values due to broadening effects. The blue shading indicates the effect of the finite radial size of the atomic wave packet σ_{rad} in $\sigma_{\mathrm{rad}}/2$ steps up to $\pm 3\sigma_{\mathrm{rad}}$ [42]. (c) Flop-flop processes versus two-atom Raman detuning $\Delta E = E_z - \Delta^\uparrow + \Delta^\downarrow$. The fit shows the characteristic sinc^2 envelope of a Fourier limited rectangular pulse with a full width half maximum FWHM $= (18.2 \pm 0.2)$ kHz. (d) Angular dependence of the flop-flop interaction at a distance of 5.6 μm.

Raman sideband cooling. This allows us to minimize the trap induced inhomogeneities by working at the lowest possible tweezer depth of $h \cdot 80$ kHz [42,43]. We then apply two-color Rydberg dressing for 50 μs, remove all $|\uparrow\rangle$ atoms by a blowout pulse, and detect remaining $|\downarrow\rangle$ atoms with a second fluorescence image. Comparing both fluorescence images allows us to infer the spin interactions by observing flipped spins and their correlations.

First, we aim to reveal the induced flop-flop interactions by choosing our detuning symmetric $\Delta^\uparrow = -\Delta^\downarrow$, to cancel flip-flop terms. We map the spatial dependence of the interactions by preparing the atoms at different distances and angles. We do not observe significant single spin flips, confirming the suppression of single-atom Raman processes. The J^{++} interaction leads to pairwise spin flips, which we observe in our setting between nearest neighbors. The distance dependence of the pairwise spin flips is shown in Fig. 3, where we scan the atoms' distances at $\theta = 90°$ and Rabi couplings of $(\Omega^\uparrow, \Omega^\downarrow) = 2\pi \cdot (0.52, 0.36)$ MHz. The experimental data and the amplitude-scaled theoretical

expectation are overall in good agreement. Differences in theory and experiment emerge from several line-broadening effects, such as the finite size of the atoms' thermal wave packet in the radial and axial direction in the traps [42], resulting in an averaging over a range of atom pair separations and angles within the radial ground state wave packet size of $\sigma^0_{\mathrm{rad}} = 0.15$ μm and the axial thermal wave packet size $\sqrt{2}\sigma^0_{\mathrm{ax}}\sqrt{k_B T/\hbar\omega_{\mathrm{ax}}} \approx 0.86$ μm for the axial trapping frequency $\omega_{\mathrm{ax}} = 2\pi \cdot 1.7$ kHz. A second effect is caused by the line shifts due to tweezer-to-tweezer inhomogeneities resulting in an average trap depth difference of $\overline{|\Delta U|} = h \cdot (10.6 \pm 1.6)$ kHz. In addition, laser phase noise currently limits the dressing time due to a twentyfold increased scattering rate appearing as atom loss [44]. We additionally map out the angular dependence of the flop-flop interaction for a fixed distance of 5.6 μm and Rabi couplings $(\Omega^{\uparrow}, \Omega^{\downarrow}) = 2\pi \cdot (0.55, 0.30)$ MHz. In this measurement, we cross a singularity in the spin-spin coupling at $\theta \approx 30°$ caused by a Rydberg pair state resonance. We reproduce a peaked interaction around this resonance, shown in Fig. 3(d), while the broadening effects explain the weak atom loss by direct Rydberg excitation on resonance [42].

In the second set of measurements, we switch on both flop-flop and flip-flop interactions by setting the detunings $(\Delta^{\uparrow}, \Delta^{\downarrow}) = 2\pi \cdot (1.4, -0.6)$ MHz and Rabi frequencies $(\Omega^{\uparrow}, \Omega^{\downarrow}) = 2\pi \cdot (0.5, 0.36)$ MHz. For the analysis, we postselect on different initial states prepared in the statistical loading of the traps (Fig. 4). The configurations of interest are either groups where two out of three tweezers at nearest neighbor distance are filled ($|\uparrow\uparrow\circ\rangle$, $|\circ\uparrow\uparrow\rangle$, where $\circ$ indicates an empty site) for the detection of flop-flop interactions or fully loaded groups ($|\uparrow\uparrow\uparrow\rangle$) for the measurement of flip-flop processes. In the latter case, assuming an initial $|\uparrow\uparrow\uparrow\rangle$ occupation, flop-flop processes introduce the $|\downarrow\rangle$ spin state, and in combination with flip-flop interactions, this leads to a detection of $|\downarrow\circ\downarrow\rangle$. We predict a different spatial dependence of J^{++} and J^{+-} [see Figs. 4(b) and 4(c)]. Note that this detection method requires flop-flop interactions to be present to initiate the dynamics out of the fully polarized initial state.

Our data reveals the angular- and distance-dependent J^{++}_{ij} interactions for an asymmetric detuning in Figs. 4(d) and 4(f). Slight discrepancies between theory and measurement may be explained by systematic errors of the imaging system calibration of less than 5%. We measure a peaked occurrence of the $|\downarrow\circ\downarrow\rangle$ pattern, which we identify as flip-flop interactions shown in Fig. 4(e). This feature reflects the tunability of our system by introducing J^{+-}_{ij} interactions for a given laser detuning, atom pair distance, and angle. In addition, we probe our system such that the flip-flop interaction strength vanishes and only flop-flop interactions occur [Figs. 4(f) and 4(g)], by scanning the angular dependence of the interactions at a fixed distance of

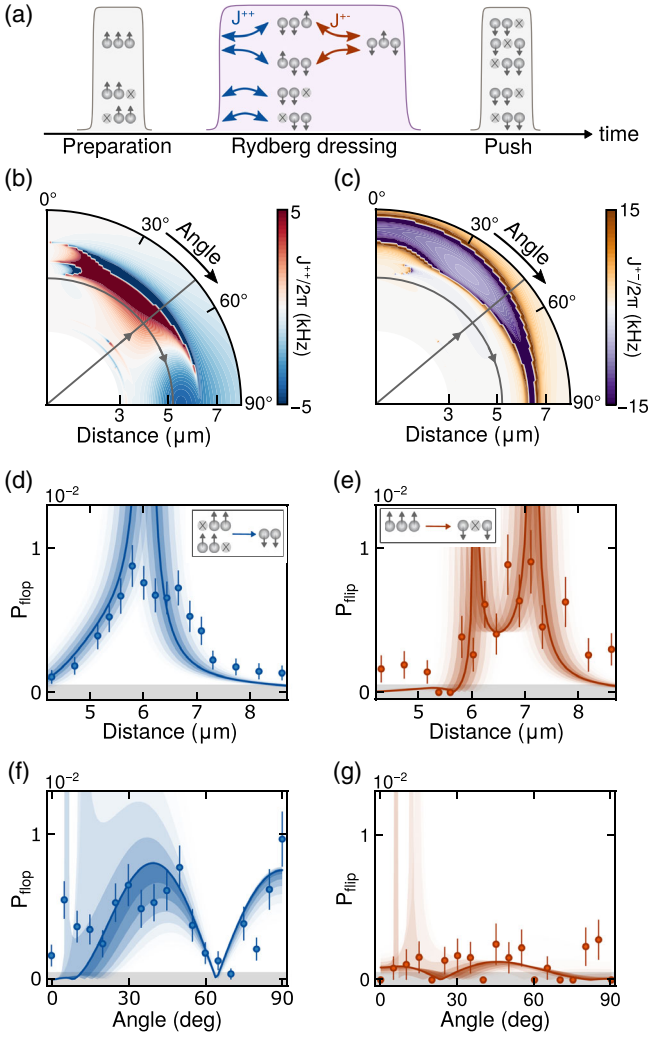

FIG. 4. Flip-flop interactions. (a) Experimental sequence. We start with optically pumping all atoms in the $|\uparrow\rangle$ state, followed by a period of Rydberg dressing and a push out pulse, leaving only atoms in the $|\downarrow\rangle$ state. We postselect two initial configurations: The atom in the center plus one additional atom or all three atoms are loaded. Depending on this configuration, flop-flop (blue arrow) and/or flip-flop processes (orange arrow) occur. (b),(c) Calculation of the distance- and angular-dependent flop-flop and flip-flop interactions. (d),(e) Distance dependence of the J^{++} and J^{+-} interactions at an angle of $\theta = 50°$ [straight gray line in (b) and (c)]. (f),(g) Angular dependence of the J^{++} and J^{+-} interactions at a distance of 5.3 μm [curved gray line in (b) and (c)]. Shadings indicate the detection limit and the effects of the spatial extension of the atomic wave packet as in Fig. 2; error bars denote 1 s.e.m.

5.3 μm without crossing a Rydberg pair resonance. The minimum in the signal, around 65°, is caused by interference on the two-atom level. Multiple Rydberg pair states $|\Psi^{(2)}_{\alpha}\rangle$ with admixtures $c^{\uparrow\uparrow}_{\alpha} c^{\downarrow\downarrow}_{\alpha}$ of opposite sign contribute such that J^{++} vanishes.

In conclusion, we have demonstrated two-color Rydberg dressing as a new technique to achieve tunable, XYZ-type

short-range spin interactions in optical tweezer arrays. Technical limitations currently prevent us from probing coherent interactions (see a more detailed discussion on the limits of the technique in the Supplemental Material [42]). The two leading limitations stem from tweezer-to-tweezer line shifts due to array inhomogeneities, and laser phase noise. None of these are fundamental, in fact, other groups have reported tweezer arrays with less than 1.1% inhomogeneity [47], a factor of 10 improvement over our arrays. Laser phase noise can be filtered by optical cavities [48] or suppressed using feed-forward techniques [49]. Beyond these issues, Doppler shifts are limiting the coherence of flop-flop interactions, which can be avoided by better Raman-sideband cooling implementable by increasing the confinement along the direction perpendicular to the tweezer plane [50]. It has been shown that the observed Rydberg pair state resonances can be utilized to enhance the coherence of Rydberg dressing [38]. By implementing these measures, we estimate that a maximum figure of merit, measured as the product of the peak interaction strength and the coherence time, of up to one hundred is reachable with current laser technology. This will allow one to realize a flexibly programmable analog quantum simulation platform for many-body quantum spin problems. Not only the ratio of the spin-interactions in the different channels can be controlled, but also the ratio of nearest- to next-nearest-neighbor interactions. This is rooted in the nonmonotonic spatial dependence of the interaction strength, which can also be used to design interactions in two dimensions for a variety of frustrated geometries [33] and static [39] or dynamic gauge fields [40].

The experimental and theoretical data and evaluation scripts that support the findings of this study are available on Zenodo [51].

This project has received funding from the European Research Council (ERC) under Grant Agreement No. 678580. We also acknowledge funding from Deutsche Forschungsgemeinschaft (GR 4741/4-1), within SPP 1929 GiRyd (GR 4741/5-1), via a Heisenberg professorship (GR 4741/3-1) and from the Alfried Krupp von Bohlen und Halbach foundation.

*lea.steinert@uni-tuebingen.de

[1] J. I. Cirac and P. Zoller, Goals and opportunities in quantum simulation, Nat. Phys. **8**, 264 (2012).
[2] I. M. Georgescu, S. Ashhab, and F. Nori, Quantum simulation, Rev. Mod. Phys. **86**, 153 (2014).
[3] C. Gross and I. Bloch, Quantum simulations with ultracold atoms in optical lattices, Science **357**, 995 (2017).
[4] M. Morgado and S. Whitlock, Quantum simulation and computing with Rydberg-interacting qubits, AVS Quantum Sci. **3**, 023501 (2021).
[5] A. M. Kaufman and K. K. Ni, Quantum science with optical tweezer arrays of ultracold atoms and molecules, Nat. Phys. **17**, 1324 (2021).
[6] H. Bernien, S. Schwartz, A. Keesling, H. Levine, A. Omran, H. Pichler, S. Choi, A. S. Zibrov, M. Endres, M. Greiner, V. Vuletić, and M. D. Lukin, Probing many-body dynamics on a 51-atom quantum simulator, Nature (London) **551**, 579 (2017).
[7] S. De Léséleuc, V. Lienhard, P. Scholl, D. Barredo, S. Weber, N. Lang, H. P. Büchler, T. Lahaye, and A. Browaeys, Observation of a symmetry-protected topological phase of interacting bosons with Rydberg atoms, Science **365**, 775 (2019).
[8] I. S. Madjarov, A. Cooper, A. L. Shaw, J. P. Covey, V. Schkolnik, T. H. Yoon, J. R. Williams, and M. Endres, An Atomic-Array Optical Clock with Single-Atom Readout, Phys. Rev. X **9**, 041052 (2019).
[9] M. A. Norcia, A. W. Young, W. J. Eckner, E. Oelker, J. Ye, and A. M. Kaufman, Seconds-scale coherence on an optical clock transition in a tweezer array, Science **366**, 93 (2019).
[10] G. Semeghini, H. Levine, A. Keesling, S. Ebadi, T. T. Wang, D. Bluvstein, R. Verresen, H. Pichler, M. Kalinowski, R. Samajdar, A. Omran, S. Sachdev, A. Vishwanath, M. Greiner, V. Vuletić, and M. D. Lukin, Probing topological spin liquids on a programmable quantum simulator, Science **374**, 1242 (2021).
[11] A. Byun, M. Kim, and J. Ahn, Finding the Maximum Independent Sets of Platonic Graphs Using Rydberg Atoms, Phys. Rev. X Quantum **3**, 030305 (2022).
[12] D. Bluvstein, H. Levine, G. Semeghini, T. T. Wang, S. Ebadi, M. Kalinowski, A. Keesling, N. Maskara, H. Pichler, M. Greiner, V. Vuletic, and M. D. Lukin, A quantum processor based on coherent transport of entangled atom arrays, Nature (London) **604**, 451 (2022).
[13] I. S. Madjarov, J. P. Covey, A. L. Shaw, J. Choi, A. Kale, A. Cooper, H. Pichler, V. Schkolnik, J. R. Williams, and M. Endres, High-fidelity entanglement and detection of alkaline-earth Rydberg atoms, Nat. Phys. **16**, 857 (2020).
[14] S. Ebadi, T. T. Wang, H. Levine, A. Keesling, G. Semeghini, A. Omran, D. Bluvstein, R. Samajdar, H. Pichler, W. W. Ho, S. Choi, S. Sachdev, M. Greiner, V. Vuletić, and M. D. Lukin, Quantum phases of matter on a 256-atom programmable quantum simulator, Nature (London) **595**, 227 (2021).
[15] P. Scholl, M. Schuler, H. J. Williams, A. A. Eberharter, D. Barredo, K. N. Schymik, V. Lienhard, L. P. Henry, T. C. Lang, T. Lahaye, A. M. Läuchli, and A. Browaeys, Quantum simulation of 2D antiferromagnets with hundreds of Rydberg atoms, Nature (London) **595**, 233 (2021).
[16] D. Bluvstein, A. Omran, H. Levine, A. Keesling, G. Semeghini, S. Ebadi, T. T. Wang, A. A. Michailidis, N. Maskara, W. W. Ho, S. Choi, M. Serbyn, M. Greiner, V. Vuletić, and M. D. Lukin, Controlling quantum many-body dynamics in driven Rydberg atom arrays, Science **371**, 1355 (2021).
[17] H. Weimer, M. Müller, I. Lesanovsky, P. Zoller, and H. P. Büchler, A Rydberg quantum simulator, Nat. Phys. **6**, 382 (2010).

[18] J. Zeiher, P. Schauß, S. Hild, T. Macrì, I. Bloch, and C. Gross, Microscopic Characterization of Scalable Coherent Rydberg Superatoms, Phys. Rev. X **5**, 031015 (2015).
[19] D. Barredo, H. Labuhn, S. Ravets, T. Lahaye, A. Browaeys, and C. S. Adams, Coherent Excitation Transfer in a Spin Chain of Three Rydberg Atoms, Phys. Rev. Lett. **114**, 113002 (2015).
[20] A. Browaeys and T. Lahaye, Many-body physics with individually controlled Rydberg atoms, Nat. Phys. **16**, 132 (2020).
[21] A. Signoles, T. Franz, R. Ferracini Alves, M. Gärttner, S. Whitlock, G. Zürn, and M. Weidemüller, Glassy Dynamics in a Disordered Heisenberg Quantum Spin System, Phys. Rev. X **11**, 011011 (2021).
[22] P. Scholl, H. J. Williams, G. Bornet, F. Wallner, D. Barredo, L. Henriet, A. Signoles, L. Henriet, T. Franz, S. Geier, A. Tebben, A. Salzinger, G. Zürn, T. Lahaye, M. Weidemüller, and A. Browaeys, Microwave-engineering of programmable XXZ Hamiltonians in arrays of Rydberg atoms, Phys. Rev. X Quantum **3**, 020303 (2022).
[23] T. Keating, R. L. Cook, A. M. Hankin, Y.-Y. Jau, G. W. Biedermann, and I. H. Deutsch, Robust quantum logic in neutral atoms via adiabatic Rydberg dressing, Phys. Rev. A **91**, 012337 (2015).
[24] Y.-Y. Jau, A. M. Hankin, T. Keating, I. H. Deutsch, and G. W. Biedermann, Entangling atomic spins with a Rydberg-dressed spin-flip blockade, Nat. Phys. **12**, 71 (2016).
[25] L. I. R. Gil, R. Mukherjee, E. M. Bridge, M. P. A. Jones, and T. Pohl, Spin Squeezing in a Rydberg Lattice Clock, Phys. Rev. Lett. **112**, 103601 (2014).
[26] J. Zeiher, R. van Bijnen, P. Schauß, S. Hild, J.-Y. Choi, T. Pohl, I. Bloch, and C. Gross, Many-body interferometry of a Rydberg-dressed spin lattice, Nat. Phys. **12**, 1095 (2016).
[27] J. Zeiher, J.-y. Choi, A. Rubio-Abadal, T. Pohl, R. van Bijnen, I. Bloch, and C. Gross, Coherent Many-Body Spin Dynamics in a Long-Range Interacting Ising Chain, Phys. Rev. X **7**, 041063 (2017).
[28] A. Arias, G. Lochead, T. M. Wintermantel, S. Helmrich, and S. Whitlock, Realization of a Rydberg-Dressed Ramsey Interferometer and Electrometer, Phys. Rev. Lett. **122**, 053601 (2019).
[29] E. Guardado-Sanchez, B. M. Spar, P. Schauss, R. Belyansky, J. T. Young, P. Bienias, A. V. Gorshkov, T. Iadecola, and W. S. Bakr, Quench Dynamics of a Fermi Gas with Strong Nonlocal Interactions, Phys. Rev. X **11**, 021036 (2021).
[30] V. Borish, O. Marković, J. A. Hines, S. V. Rajagopal, and M. Schleier-Smith, Transverse-Field Ising Dynamics in a Rydberg-Dressed Atomic Gas, Phys. Rev. Lett. **124**, 063601 (2020).
[31] S. Hollerith, K. Srakaew, D. Wei, A. Rubio-Abadal, D. Adler, P. Weckesser, A. Kruckenhauser, V. Walther, R. van Bijnen, J. Rui, C. Gross, I. Bloch, and J. Zeiher, Realizing Distance-Selective Interactions in a Rydberg-Dressed Atom Array, Phys. Rev. Lett. **128**, 113602 (2022).
[32] S. Weber, C. Tresp, H. Menke, A. Urvoy, O. Firstenberg, H. P. Büchler, and S. Hofferberth, Calculation of Rydberg interaction potentials, J. Phys. B **50**, 133001 (2017).
[33] A. W. Glaetzle, M. Dalmonte, R. Nath, C. Gross, I. Bloch, and P. Zoller, Designing Frustrated Quantum Magnets with Laser-Dressed Rydberg Atoms, Phys. Rev. Lett. **114**, 173002 (2015).
[34] P. Schauß, J. Zeiher, T. Fukuhara, S. Hild, M. Cheneau, T. Macrì, T. Pohl, I. Bloch, and C. Gross, Crystallization in Ising quantum magnets, Science **347**, 1455 (2015).
[35] V. Lienhard, S. De Léséleuc, D. Barredo, T. Lahaye, A. Browaeys, M. Schuler, L. P. Henry, and A. M. Läuchli, Observing the Space- and Time-Dependent Growth of Correlations in Dynamically Tuned Synthetic Ising Models with Antiferromagnetic Interactions, Phys. Rev. X **8**, 021070 (2018).
[36] K. Kim, M. S. Chang, S. Korenblit, R. Islam, E. E. Edwards, J. K. Freericks, G. D. Lin, L. M. Duan, and C. Monroe, Quantum simulation of frustrated Ising spins with trapped ions, Nature (London) **465**, 590 (2010).
[37] A. Periwal, E. S. Cooper, P. Kunkel, J. F. Wienand, E. J. Davis, and M. Schleier-Smith, Programmable interactions and emergent geometry in an array of atom clouds, Nature (London) **600**, 630 (2021).
[38] R. M. W. van Bijnen and T. Pohl, Quantum Magnetism and Topological Ordering via Rydberg Dressing near Förster Resonances, Phys. Rev. Lett. **114**, 243002 (2015).
[39] X. Wu, F. Yang, S. Yang, K. Mølmer, T. Pohl, M. K. Tey, and L. You, Manipulating synthetic gauge fluxes via multicolor dressing of Rydberg-atom arrays, Phys. Rev. Res. **4**, L032046 (2022).
[40] P. S. Tarabunga, F. M. Surace, R. Andreoni, A. Angelone, and M. Dalmonte, Gauge-Theoretic Origin of Rydberg Quantum Spin Liquids, Phys. Rev. Lett. **129**, 195301 (2022).
[41] D. Sels and E. Demler, Quantum generative model for sampling many-body spectral functions, Phys. Rev. B **103**, 014301 (2021).
[42] See Supplemental Material at http://link.aps.org/supplemental/10.1103/PhysRevLett.130.243001 for detailed derivation of the interactions and discussion of the technical limitations, which includes Refs. [32,33,38,43–46].
[43] N. Lorenz, L. Festa, L.-M. Steinert, and C. Gross, Raman sideband cooling in optical tweezer arrays for Rydberg dressing, SciPost Phys. **10**, 52 (2021).
[44] L. Festa, N. Lorenz, L.-M. Steinert, Z. Chen, P. Osterholz, R. Eberhard, and C. Gross, Blackbody-radiation-induced facilitated excitation of Rydberg atoms in optical tweezers, Phys. Rev. A **105**, 013109 (2022).
[45] N. R. Hutzler, L. R. Liu, Y. Yu, and K.-K. Ni, Eliminating light shifts for single atom trapping, New J. Phys. **19**, 023007 (2017).
[46] A. Urvoy, F. Ripka, I. Lesanovsky, D. Booth, J. P. Shaffer, T. Pfau, and R. Löw, Strongly Correlated Growth of Rydberg Aggregates in a Vapor Cell, Phys. Rev. Lett. **114**, 203002 (2015).
[47] D. Kim, A. Keesling, A. Omran, H. Levine, H. Bernien, M. Greiner, M. D. Lukin, and D. R. Englund, Large-scale uniform optical focus array generation with a phase spatial light modulator, Opt. Lett. **44**, 3178 (2019).
[48] H. Levine, A. Keesling, A. Omran, H. Bernien, S. Schwartz, A. S. Zibrov, M. Endres, M. Greiner, V. Vuletić, and M. D. Lukin, High-Fidelity Control and Entanglement of Rydberg-Atom Qubits, Phys. Rev. Lett. **121**, 123603 (2018).

[49] L. Li, W. Huie, N. Chen, B. DeMarco, and J. P. Covey, Active Cancellation of Servo-Induced Noise on Stabilized Lasers via Feedforward, Phys. Rev. Appl. **18**, 064005 (2022).

[50] A. W. Young, W. J. Eckner, W. R. Milner, D. Kedar, M. A. Norcia, E. Oelker, N. Schine, J. Ye, and A. M. Kaufman, Half-minute-scale atomic coherence and high relative stability in a tweezer clock, Nature (London) **588**, 408 (2020).

[51] L.-M. Steinert, P. Osterholz, R. Eberhard, L. Festa, N. Lorenz, Z. Chen, A. Trautmann, and C. Gross, Spatially programmable spin interactions in neutral atom arrays, Zenodo, 10.5281/zenodo.6906497 (2022).